Available online at www.sciencedirect.com
SCIENCE DIRECT®
Journal of Sound and Vibration 279 (2005) 327–344
JOURNAL OF SOUND AND VIBRATION
www.elsevier.com/locate/jsvi

Non-linear dynamics and chaos control for an electromagnetic system

Shun-Chang Chang*, Hai-Ping Lin

Department of Mechanical and Automation Engineering, Da-Yeh University, 112 Shan-Jiau Road, Da-Tsuen, Chang-Hua Taiwan 51505, ROC

Received 7 May 2003; accepted 6 November 2003

Abstract

A non-linear mathematical model has been obtained by applying a modified conventional identification technique based on the principle of harmonic balance. In this study, analytical work is carried out on this identified non-linear model by applying the first-harmonic approximation solution and the Floquet theory. The resulting criteria for bifurcations can be used to evaluate the operational range of a system employing such a non-linear actuator. We also employ the method of Lyapunov exponents to show the occurrence of chaotic motion and to verify the above analyses. Finally, various methods, such as the state feedback control and injection of dither signal control are used to control chaos effectively.

1. Introduction

It is well known that the characteristics of magnetic bearings are inherently non-linear due to the non-linearities of electromagnetic forces. To accurately control or predict the performance of this system, the effects of these non-linearities must be taken into consideration. Therefore, in our previous work [1], an experiment with a symmetric rotor with a spring device, as shown in Fig. 1, was carried out by applying a series of non-linear electromagnetic forces to identify a non-linear model for the system.

For easy reference, the experimental results presented in the previous work are repeated here. Fig. 2 shows the frequency responses of the rotor displacement for an input amplitude $p_0 = 3.0$ V in decreasing forcing frequency (ω) from 80 to 34.4 Hz. It can be seen that if the system starts at high frequency and the forcing frequency is slowly decreased, there is an increase in amplitude

*Corresponding author. Fax: +886-4-851-1224.
E-mail address: changsc@mail.dyu.edu.tw (S.-C. Chang).

0022-460X/$ - see front matter
doi:10.1016/j.jsv.2003.11.033

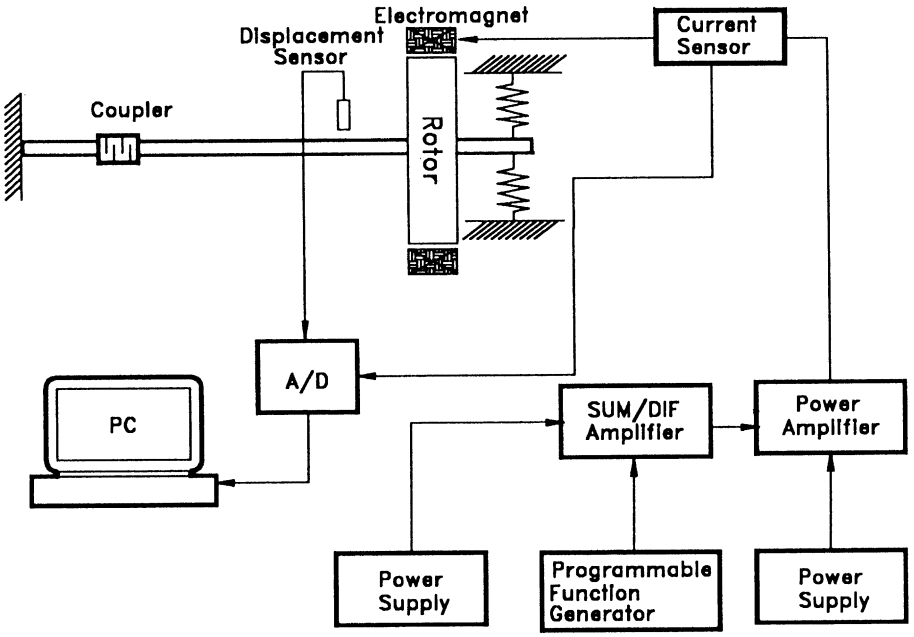

Fig. 1. Schematic diagram of the electromagnetic system.

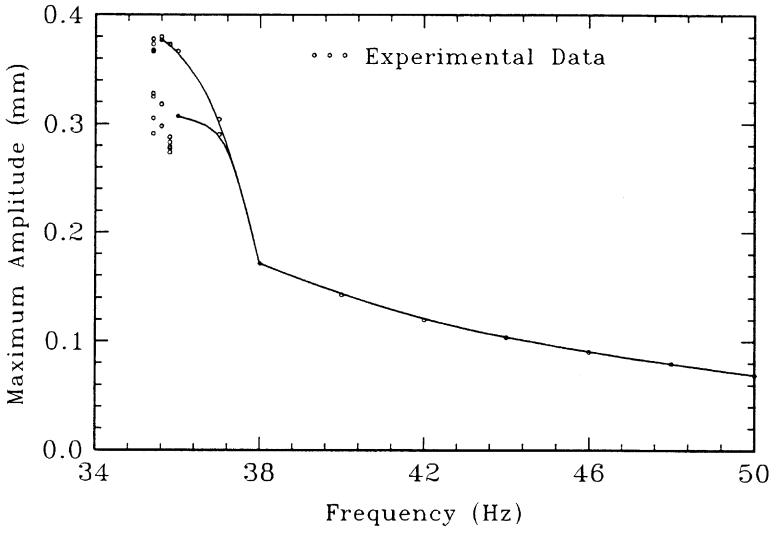

Fig. 2. Bifurcation diagram obtained from the experiment.

along the resonant part of the response curve. The smooth variations in amplitude and frequency continue until $\omega = 37.6$ Hz, where the first period-doubling bifurcation occurs. In this type of period-doubling bifurcation a stable limit cycle loses its stability, while another closed orbit is

born whose period is twice the period of the original oscillation. Beyond this point, the vibrating amplitude of the rotor and the coil current grow sharply. As the forcing frequency continues to decrease, the trajectory continues to experience period-doubling bifurcations, which eventually result in likely chaotic motion, and finally the rotor strikes the electromagnet, i.e., the system blows up.

This shows that the system exhibits complicated non-linear behavior due to the non-linearities of the electromagnetic force. In engineering applications, this should be taken into consideration at the design stage.

To study the dynamics of this system further we have modified the conventional identification technique based on the principle of harmonic balance to identify this system. The resulting non-linear model [1] is obtained as

$$\frac{\mathrm{d}^2y}{\mathrm{d}t^2} + b_1\frac{\mathrm{d}y}{\mathrm{d}t} + b_2y + b_3y^2 + b_4y^3,$$

$$b_5(I_0+i)^{6/3} + b_6(I_0+i)^{2/3} + b_7(I_0+i)^{4/3} + b_0 = 0, \tag{1a}$$

$$L_1(I_0+i)^{-1}\frac{\mathrm{d}i}{\mathrm{d}t} + iR = K_A p_0 \sin\omega t, \tag{1b}$$

where I_0 is the biased current calculated directly from the average experimental current time series, i is the oscillating current about I_0 ($= 0.68$ A), y is the oscillating displacement of the rotor about a reference point, R is the resistance of the coil, and K_A ($= 2.254$) is the power amplifier gain. The other necessary coefficients for Eqs. (1) are listed in Table 1.

This model successfully captures the primary characteristics of the system by comparing the frequency responses from simulations to those from experiments. However, theoretical analyses of this model showing whether the identified non-linear mathematical model obtained from the experiment can predict and characterize the dynamics of the real system have not yet been carried out. Furthermore, the occurrence of chaotic motion at the moment the rotor strikes the electromagnet has also not been undertaken.

In this study, analytical work is performed for this identified model using the first-harmonic approximation solution and the Floquet theory [2]. The method of Lyapunov exponents [3] is also applied to show the occurrence of chaotic motion and the resulting criteria for bifurcations are used to compare with those obtained from the Floquet theory and experimental results to prove the effectiveness of the analysis.

In many engineering problems of chaos control it is important to develop control techniques to drive a chaotic attractor to a periodic orbit. Since the pioneering work of Ott et al. [4] in controlling chaos, many modified methods and other approaches have successively been proposed [5–10]. Finally, in order to improve the performance of a dynamics system or avoid the chaotic behavior, sometimes we have to convert a chaotic behavior into a periodic motion. Various methods are presented to control chaos: the state feedback control [8,9] and application of dither signal control [10].

Table 1
Identified results

System parameter	Identified value
b_1	43.843782
b_2	1.7461747×10^4
b_3	3.969473×10^4
b_4	-16.80843×10^4
b_5	3.3106×10^4
b_6	10.505×10^4
b_7	-9.98479×10^4
b_0	-3.443392×10^4
L_1	0.018096
R	9.7922279

2. Stability and bifurcation analysis

To perform the bifurcation analysis, we derive approximate periodic solutions for Eqs. (1) and examine their instability by considering the variational Hill type equation [11]. For convenience, we first let $\omega_n = \sqrt{b_2}$, $\Omega = \omega/\omega_n$ and $\tau = \omega_n t$, and normalize Eqs. (1) to the form

$$\frac{d^2y}{d\tau^2} + \left(\frac{b_1}{\omega_n}\right)\frac{dy}{d\tau} + y + \frac{(b_3y^2 + b_4y^3 + b_5(I_0+i)^{6/3} + b_6(I_0+i)^{2/3} + b_7(I_0+i)^{4/3} + b_0)}{\omega_n^2} = 0, \quad (2a)$$

$$\frac{di}{d\tau} = \frac{(K_A p_0 \sin\Omega\tau - iR)(I_0+i)}{L_1\omega_n}. \quad (2b)$$

To facilitate the calculations, the non-linear terms in Eqs. (2) are expanded in a Taylor series and truncated at the fourth order, i.e.,

$$\frac{d^2y}{d\tau^2} + 0.33179\frac{dy}{d\tau} + y + 2.27324y^2 - 9.62586y^3 + 0.43493i, - 0.86517i^2 + 1.26763i^3 - 0.95581i^4 + 0.13755 = 0, \quad (3a)$$

$$\frac{di}{d\tau} = \frac{(2.254p_0\sin(\Omega\tau) - 9.79i)(I_0+i)}{\omega_n L_1}. \quad (3b)$$

With this equation, we can employ the harmonic balance method [2] to approximate a periodic solution for this system. Because Eqs. (1) are unsymmetrical, solutions for this system will also be unsymmetrical. Such unsymmetrical solutions may simultaneously contain a constant term and both even and odd harmonics. Generally, when the system is operated in the region of the principal resonance, the lowest harmonic may dominate the amplitude of the response. Those harmonics with higher frequencies are relatively small and such that the effects of the higher harmonics can be neglected. Thus, the solutions for Eqs. (3) are assumed to be

$$y(\tau) = A_0 + A_1\cos(\Omega\tau + \theta_1), \quad (4)$$

$$i(\tau) = B_0 + B_1\cos(\Omega\tau + \theta_2). \quad (5)$$

Substituting Eqs. (4) and (5) into Eqs. (3), neglecting the higher harmonic terms and matching coefficients of $\sin(\Omega\tau)$, $\cos(\Omega\tau)$, and the constant term to zero, we obtain a set of algebraic equations for the unknown parameters $A_0, A_1, \theta_1, B_0, B_1, \theta_2$ as follows:

$$G_1\cos(\theta_1) + G_2\sin(\theta_1) + G_3\cos(\theta_2) = 0, \tag{6}$$

$$G_2\cos(\theta_1) - G_1\sin(\theta_1) - G_3\sin(\theta_2) = 0, \tag{7}$$

$$F_1\cos(\theta_2) + F_2\sin(\theta_2) = 0, \tag{8}$$

$$F_0 + F_2\cos(\theta_2) - F_1\sin(\theta_2) = 0, \tag{9}$$

$$H_0 + H_1\sin(\theta_2) = 0, \tag{10}$$

$$J = 0, \tag{11}$$

where $G_1, G_2, G_3, F_0, F_1, F_2, H_0, H_1, J$ are all functions of $A_0, A_1, \theta_1, B_0, B_1, \theta_2, \Omega, p_0$, which are shown in Appendix A. By performing numerical calculations, Eqs. (6)–(11) can be solved simultaneously.

With the approximate solutions for Eqs. (3) at hand, we are ready to examine the local stability of the solutions using the Floquet theory [2]. To proceed, we consider the perturbed solution as [12–15]

$$\tilde{y}(\tau) = y(\tau) + \delta y(\tau), \tag{12}$$

where δy represents a small perturbation. Because the current i in Eq. (2b) is independent of rotor displacement and the bifurcations for i were never seen to occur in the experiment, the assumed solution (5) is unperturbed for the following analysis. Inserting the above perturbed solution into Eqs. (3), employing the assumed solutions $y(\tau)$ and $i(\tau)$ in Eqs. (4) and (5) and noting that δy is relatively small, the perturbation δy is then governed by the linearized variational equation

$$\frac{\mathrm{d}^2\delta y}{\mathrm{d}\tau^2} + 0.33179\frac{\mathrm{d}\delta y}{\mathrm{d}\tau} + (\bar{\lambda}_0 + \bar{\lambda}_1\cos(\Omega\tau + \theta_1) + \bar{\lambda}_2\cos(2\Omega\tau + 2\theta_1))\delta y = 0, \tag{13}$$

where the coefficients $\bar{\lambda}_{0-2}$ are functions of $A_0, A_1, \theta_1, B_0, B_1, \theta_2, \Omega, p_0$ and are shown in Appendix A. The higher order harmonics have been truncated.

Eq. (13) is clearly a Hill's type equation. With this equation, the behavior of the perturbation δy with time and hence the stability of the harmonic solution (4) can be examined straightforwardly. Eq. (13) has two parametric excitations: $\cos(\Omega\tau + \theta_1)$ and $\cos(2\Omega\tau + 2\theta_1)$, with driven frequencies Ω and 2Ω, respectively. The Floquet theory [2] suggests that a system driven parametrically may exhibit resonance whenever the driven frequencies are equal to $2\sqrt{\bar{\lambda}_0}/k$, where k is an integer and $\sqrt{\bar{\lambda}_0}$ represents the normalized natural frequency of Eq. (13). In the A_1-Ω plane, these resonance conditions represent the points along the Ω axis from which the unstable regions emanate. For our system, $k = 1$, the so-called first order instability, is of interest.

For the excitation $\cos(\Omega\tau + \theta_1)$, the instability can occur close to $\Omega \approx 2\sqrt{\bar{\lambda}_0}$. This type of instability is helpful in predicting the occurrence of period-doubling bifurcations. The central ideal is that any parametric term in the linearized variational equation with a period, which is the same

as that of the assumed solution, could give rise to the appearance of a new subharmonic component having twice the period of the assumed solution. On the other hand, the excitation $\cos(2\Omega\tau + 2\theta_1)$ leads to the stability limit, i.e., the so-called jump phenomenon, when $\Omega \approx \sqrt{\bar{\lambda}_0}$. Such an instability coincides with the point of the vertical tangents on the resonance curves $A_1(\Omega)$ and $A_0(\Omega)$. In our system, this is unlikely to occur, because it only appears period-doubling bifurcation from experimental data (as shown in Fig. 2). The system may have blown up before entering this instability limit.

In light of the above and according to the Floquet theory, inside the unstable region solutions for Eq. (13) with a period T_f or $2T_f$ ($T_f = 2\pi/\Omega$) are possible [12,15]. That is,

$$\delta y = \mathrm{e}^{\varepsilon\tau}\phi(\tau). \tag{14}$$

When $\varepsilon = 0$ is at the stability limit, and $\phi(\tau)$ is a periodic function with period T_f or $2T_f$. In the case where $\phi(\tau)$ is assumed to have period T_f, it simply leads to the jump phenomenon. On the other hand, when $\phi(\tau)$ is assumed to have period $2T_f$, we can predict the occurrence of period-doubling bifurcation. We recall that the approximate theory of Hill's equations allows one to assume functions $\phi(\tau)$ as a truncated Fourier series. Hence, at the stability limits, the first approximation solution of perturbation δy can be assumed as

$$\delta y = \mathrm{e}^{\varepsilon\tau}\left(C_0 + C_1\cos\left(\frac{\Omega}{2}\tau + \vartheta_1\right)\right), \tag{15}$$

and at the stability limit ($\varepsilon = 0$), δy becomes

$$\delta y = C_0 + C_1\cos\left(\frac{\Omega}{2}\tau + \vartheta_1\right). \tag{16}$$

Substituting Eq. (16) into Eq. (13) and applying the method of harmonic balance, one finds that for C_0, C_1 and ϑ_1 to be non-trivial, the following condition must be satisfied:

$$F_c(\Omega, p_0) = 5.167A_1^2 - 131.29A_0A_1^2 + 833.914A_0^2A_1^2 - 0.0275\Omega^2 - \frac{\Omega^4}{16} = 0. \tag{17}$$

Using criterion (17) and Eqs. (6)–(11), all of the period-doubling bifurcation points corresponding to various values of p_0 and Ω can be predicted by numerical calculations [12]. As an example, for $p_0 = 3.0$ V, the combination of Eqs. (17) and (6)–(11) predicts that the resonance curve A_1 first enters the unstable region at $\Omega = 1.812$ in decreasing the driving frequency, which is the first period-doubling bifurcation point.

From the engineering point of view, criterion (17) is practical in the design stage, because beyond this bifurcation point the oscillating amplitude increases rapidly with decreasing forcing frequency. Within a considerable narrow range of forcing frequency, the system consequently leads to chaotic motion with relatively large amplitude and finally blows up. Thus, the first period-doubling bifurcation point can be treated as an operational limit in frequency for this system. The results of the analytical analysis are useful at the design stage to evaluate the operational range for systems utilizing a non-linear electromagnet as an actuator.

3. Lyapunov exponent and Lyapunov dimension

The analyses presented in Section 2 show the possibility for the identified model to exhibit period-doubling bifurcations, and it can serve to predict the points where the first period-doubling bifurcation occurs. However, a likely chaotic motion exhibited in the experiment is still unable to be ascertained. In this section, the method of Lyapunov exponents is applied to verify the occurrence of chaotic motion for the identified model.

For every dynamic system, there is a spectrum of Lyapunov exponents (λ) [3] that tells how length, areas and volumes change in phase space. As a criterion for the existence of chaos, one needs only to calculate the largest exponent, which tells whether nearby trajectories diverge ($\lambda > 0$) or converge ($\lambda < 0$) on average. Any bounded motion in a system containing at least one positive Lyapunov exponent is defined as chaotic, while for periodic motion, the Lyapunov exponents are not positive.

Referring to the algorithm for calculating the Lyapunov exponents described by Wolf et al. [3], the evolution of the largest Lyapunov exponent for $p_0 = 3.0$ V is computed as displayed in Fig. 3. From this figure, we find that the onset of chaotic motion is at $\Omega = 1.710$, because at this point, P_4, the largest Lyapunov exponent, changes its sign from negative to positive when the normalized forcing frequency is slowly decreased. For points P_{1-3}, the largest Lyapunov exponents are shown to approach zero. The system at these points may undergo bifurcations. However, the Lyapunov exponent at such a point provides no means to determine the type of bifurcation, so more advanced tools such as those presented in Section 2 must be applied. For example, the analysis in Section 2 predicts the occurrence of the first period-doubling bifurcation at $\Omega = 1.812$, while point P_1, where the largest Lyapunov exponent first approaches zero, is found at $\Omega = 1.8475$.

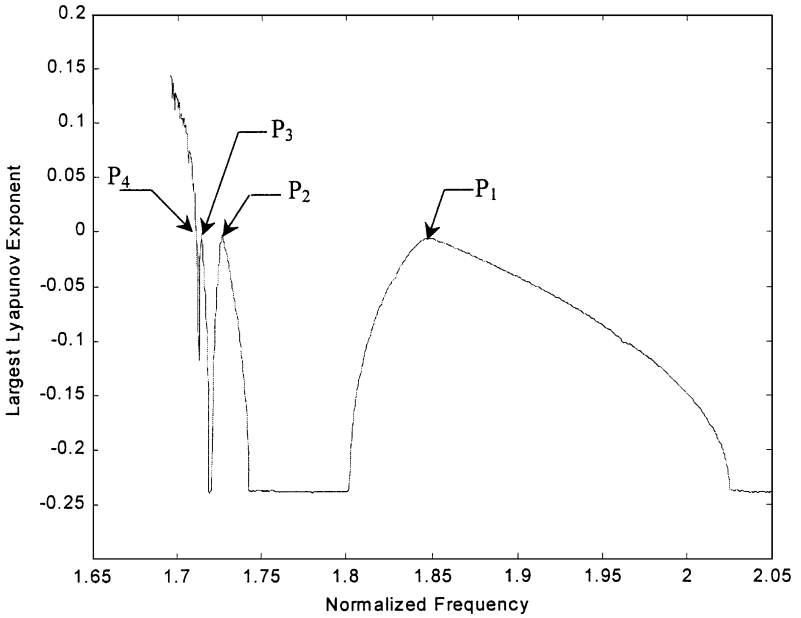

Fig. 3. The largest Lyapunov exponents of the system for $p_0 = 3.0$ V.

When the forcing frequency is larger than P_1, $\Omega = 1.95$; as an example, the Lyapunov exponents computed from Eqs. (2) are $\lambda_1 = -0.082501$, $\lambda_2 = -0.396172$, and $\lambda_3 = -4.017426$. Their sum $\lambda_1 + \lambda_2 + \lambda_3 = -4.496099$, which is negative, showing that the motion of the rotor at these values finally converges to a stable limit cycle. Indicating with $\lambda_1 \geqslant \cdots \geqslant \lambda_n$ the Lyapunov exponents of a dynamical system, Kaplan and Yorke [16] provide an estimation for the Lyapunov dimension d_L as

$$d_L = j + \frac{1}{|\lambda_{j+1}|}\sum_{i=1}^{j} \lambda_i, \tag{18}$$

where j is the largest integer that satisfies $\sum_{i=1}^{j} \lambda_i > 0$. By applying the technique, the Lyapunov dimension of Eqs. (2) for $\Omega = 1.95$ is $d_L = 1$. Because the value of the Lyapunov dimension is an integer, the system has a periodic motion. When the forcing frequency Ω decreases across the bifurcation point, for example $\Omega = 1.708$, the Lyapunov exponents are $\lambda_1 = 0.1447$, $\lambda_2 = -0.6234$ and $\lambda_3 = -4.01773$. Here, the Lyapunov dimension is $d_L = 2.232$. It should be noted that the value of the Lyapunov dimension is not an integer; the system at this point can process fractal basin boundaries [14]. This reveals that a measure of the fractal geometry of the attractor and the property of sensitivity dependence on initial conditions exist in the system. Fig. 4 shows the fractal basin boundaries in such a case, with fixed $p_0 = 3.0$ V, $\Omega = 1.708$ and various initial conditions. For calculation [13], 1600×250 sets of initial conditions were chosen in the form of a grid, and integration of Eqs. (2) using a fifth order Runge–Kutta integration algorithm was continued until the system either converged to the bounded attractors or diverged. Initial conditions in the light regions lead to the divergent solutions, while the dark regions are the basins for the bounded attractors. The fractal structure points out that small uncertainties in the initial conditions can lead to unpredictability of the system output.

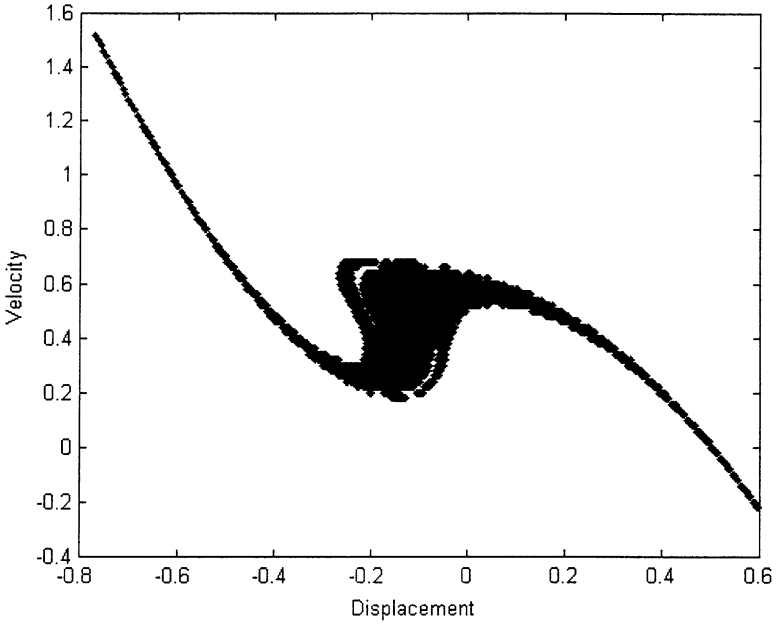

Fig. 4. Fractal basin boundaries of the system for $p_0 = 3.0$ V at $\Omega = 1.708$.

4. Simulations and discussions

To clearly understand the characteristics of this system, we carry out a series of numerical simulations from Eqs. (2). The commercial package DIVPRK of IMSL [17] in FORTRAN subroutines for mathematics applications is used to solve ordinary differential equations. The resulting bifurcation diagram is shown in Fig. 5. It can be clearly seen from this figure that the first period-doubling bifurcation occurs at about $\Omega = 1.863$, and that at $\Omega = 1.715$ chaotic motion appears. More details about the various responses exhibited by the system are presented in Fig. 6. There, each type of response is characterized by a Poincaré map (Poincaré velocity vs. phase angle) and frequency spectrum. Figs. 6(a) and (b) show that the T_f-period mainly involves the constant term and the fundamental components. From Figs. 6(c) and (d), we find that a cascade of period-doubling bifurcations causes a series of subharmonic components, which show the bifurcations with new frequency components at $\Omega/2$, $3\Omega/2$, $5\Omega/2, \ldots$. The particular features of two descriptors characterize the essence of the chaotic behavior: the Poincaré map and the frequency spectrum. The Poincaré map shows an infinite set of points referred to as a "strange attractor". Simultaneously, the frequency spectrum of chaotic motion is a continuous broad spectrum. The two features—"strange attractor" and continuous type Fourier spectrum—are strong indicators of chaos. Chaotic motions are shown in Figs. 6(g) and (h).

It is clearly shown that the simulating results are quite in agreement with the analysis in the previous sections.

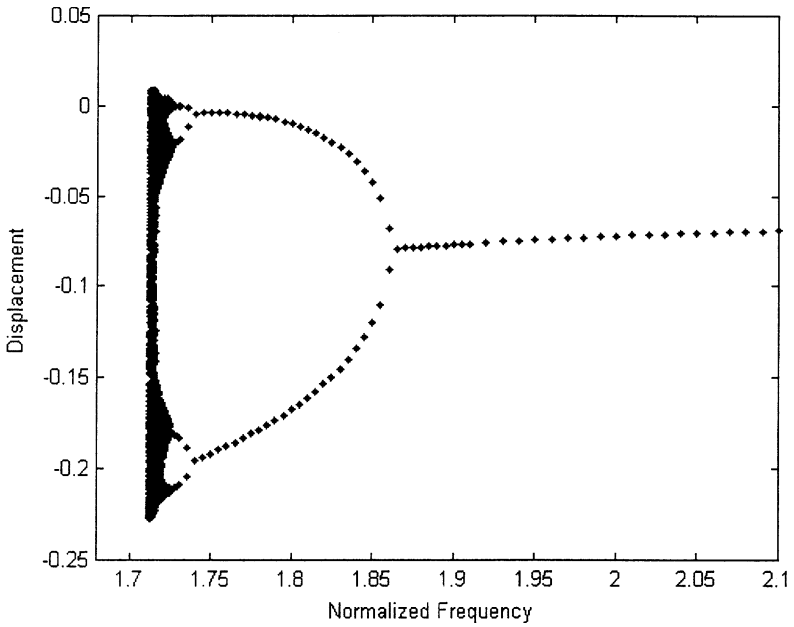

Fig. 5. Bifurcation diagram of the system for $p_0 = 3.0$ V.

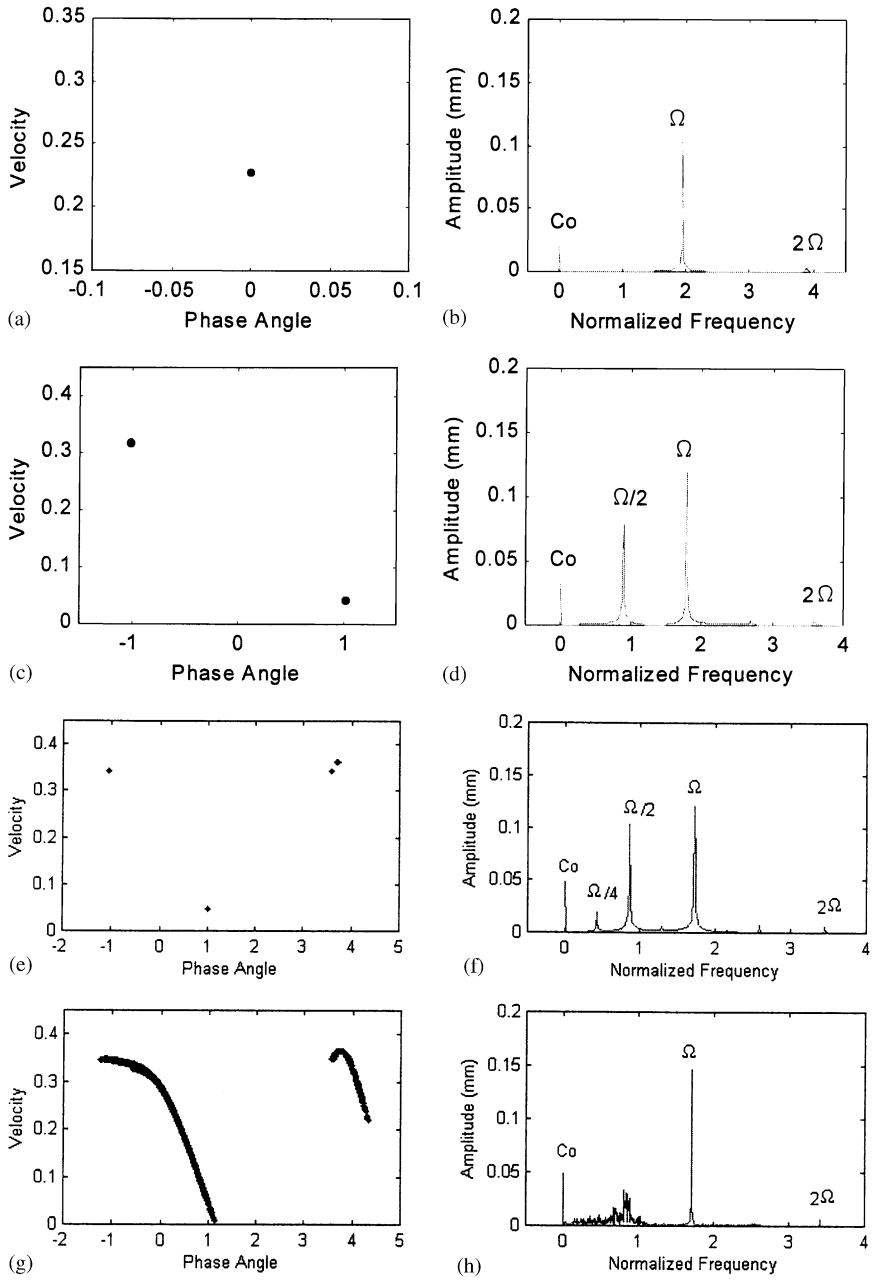

Fig. 6. Frequency spectra and Poincaré maps of various responses of numerical simulations for $p_0 = 3.0$ V: (a) and (b) period-one motion, $\Omega = 1.95$; (c) and (d) period-two motion, $\Omega = 1.80$; (e) and (f) period-four motion, $\Omega = 1.7255$; (g) and (h) chaotic motion, $\Omega = 1.708$.

5. Controlling chaos

Analyzing and predicting the behaviors of a chaotic system is beneficial, but to maximize the benefit, one has to be able to control it. In order to improve the performance of a dynamic system or avoid the chaotic phenomena, we must convert a chaotic behavior into a desired stable periodic motion.

In this section, we discuss how chaos can be converted into periodic motion by minimal efforts. Two methods, which are used to control chaos, will be presented: the addition of state feedback control [8,9], the addition of dither signals [10].

5.1. State feedback control

Recently, Cai et al. [8,9] have suggested a simple and effective state feedback control algorithm. This method can be explained briefly: consider the n-dimensional dynamical system

$$\dot{x} = f(x, t), \tag{19}$$

where $x(t) \in R^n$ is the state vector and $f = (f_1, \ldots, f_i, \ldots, f_n)$, where f_i is a linear or a non-linear function and f includes at least one non-linear function. Suppose $f_k(x, t)$ is the key non-linear function that leads to chaotic motion in system (19); then only one term of state feedback of an available system variable x_m is added to the equation that includes $f_k(x, t)$ as follows:

$$\dot{x}_k = f_k(x, t) + Px_m, \quad k, m \in \{1, 2, \ldots, n\}, \tag{20}$$

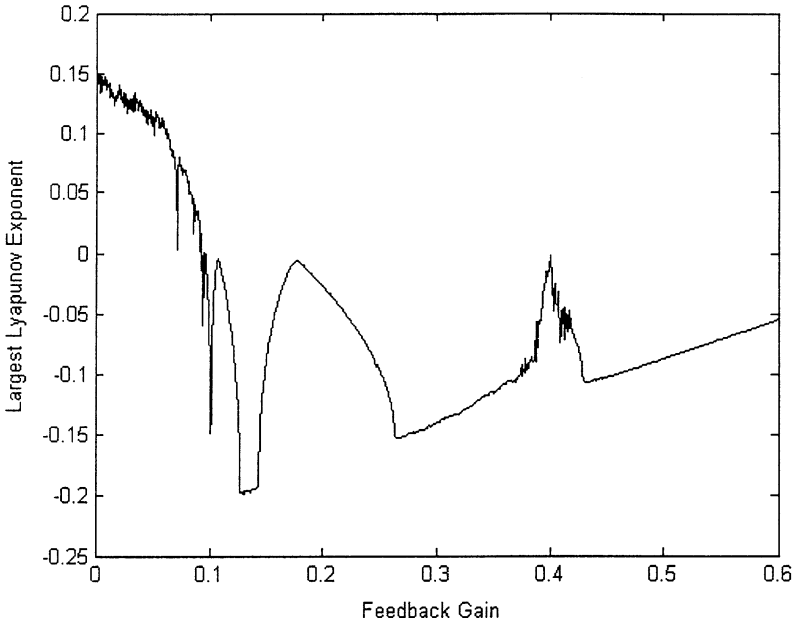

Fig. 7. Maximum Lyapunov exponents versus feedback gains.

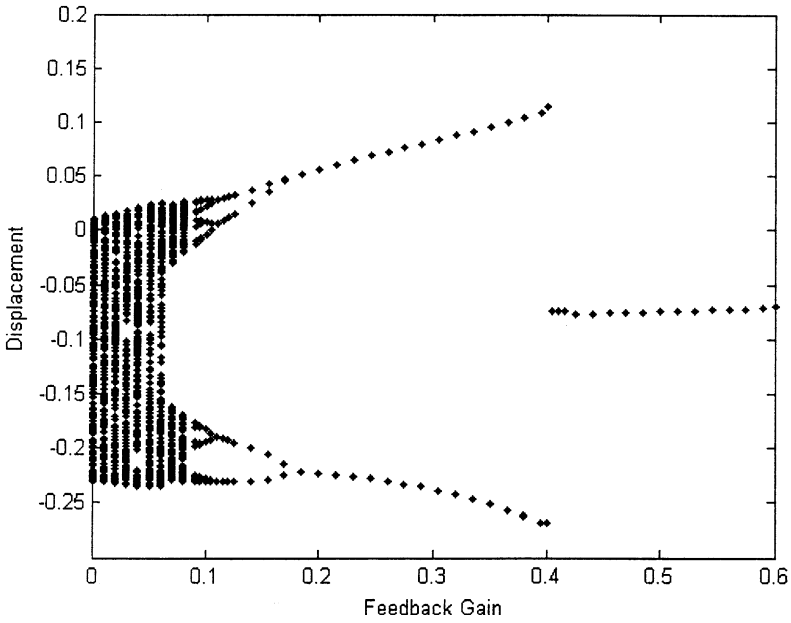

Fig. 8. Bifurcation diagram for feedback gains (P) between 0 and 0.6.

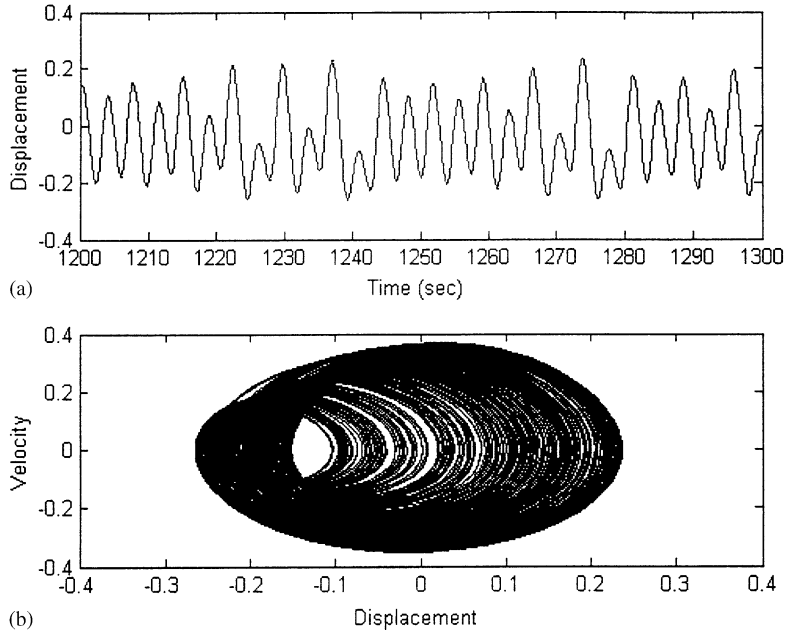

Fig. 9. Chaotic motion of the uncontrolled system ($P = 0.0$): (a) time response; (b) phase portrait.

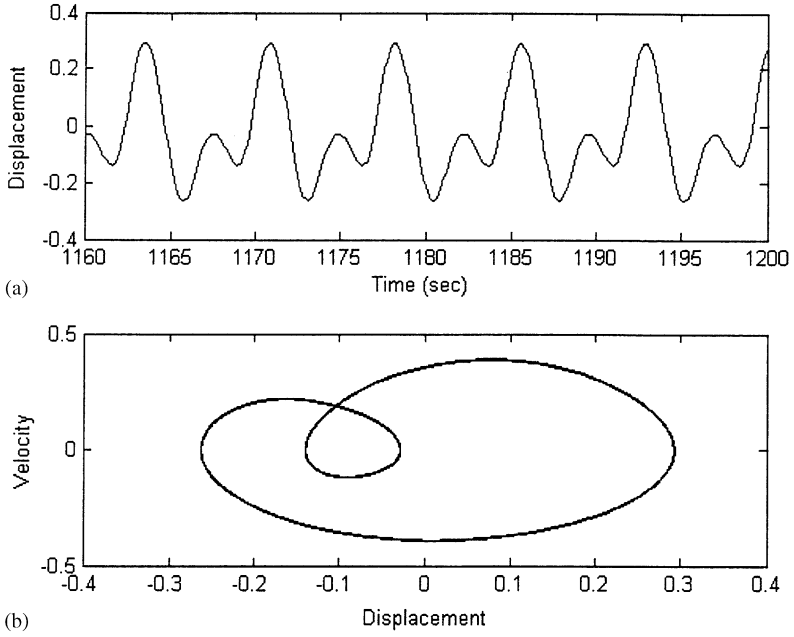

Fig. 10. Period-two motion of the system with state feedback control ($P = 0.2$): (a) time response; (b) phase portrait.

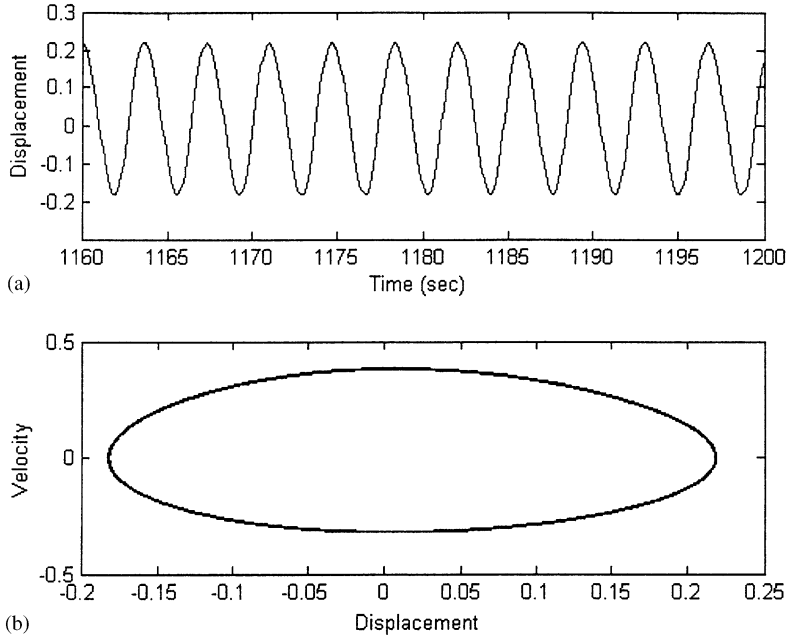

Fig. 11. Period-one motion of the system with state feedback control ($P = 0.5$): (a) time response; (b) phase portrait.

where P is feedback gain. Other functions keep their original forms. In order to understand this simple controlling approach in a better way, this method is applied to Eqs. (2) numerically.

In the absence of the state feedback control, Eqs. (2) exhibit chaotic behavior under the parameters $A_0 = 3.0$ V and $\Omega = 1.708$. Consider the effect of the state feedback control added to the right-hand side of the Eq. (2b). By increasing the feedback gain P from 0 to 0.75, the chaotic behavior disappears. The evolution of the largest Lyapunov exponent for $A_0 = 3.0$ V and $\Omega = 1.708$ is shown in Fig. 7. The resulting bifurcation diagram is shown in Fig. 8. It can be clearly seen from those two figures that the chaotic motion exists in the region between $P = 0$ and $P = 0.092$. When $P = 0$, Eqs. (2) displays chaotic motion (see Figs. 9). When $P = 0.2$, a period-2 orbit (see Figs. 10) exists in Eqs. (2). And the period-1 orbit in Eqs. (2) with $P = 0.5$ is shown in Figs. 11. In further simulations, when $0.10 < P < 0.75$, Eqs. (2) exhibit low-periodic orbits.

Therefore, in order to suppress the occurrence of chaos, simple state feedback of a system variable can be enough to disturb the balance of dynamical behavior in the chaotic system.

5.2. Dither control

Using the dither signal method, we can convert a chaotic motion to a periodic orbit or a steady state motion dependent on the system input. Let us add a square-wave dither signal W in front of the non-linearity $f(.)$. Thus, f has the effective value output:

$$\mu = \tfrac{1}{2}[f(y + W) + f(y - W)]. \tag{21}$$

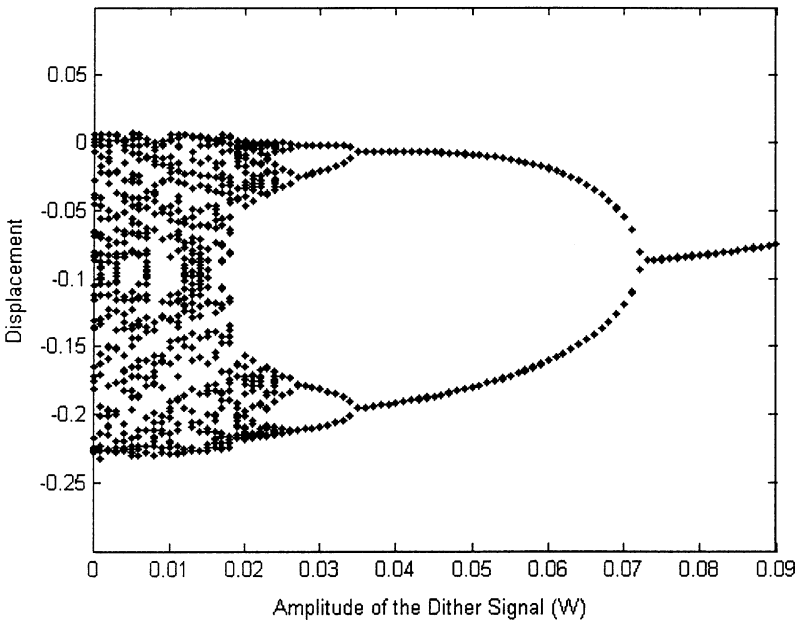

Fig. 12. Bifurcation diagram of the system with a square-wave dither, where W denotes the amplitude of the dither signal.

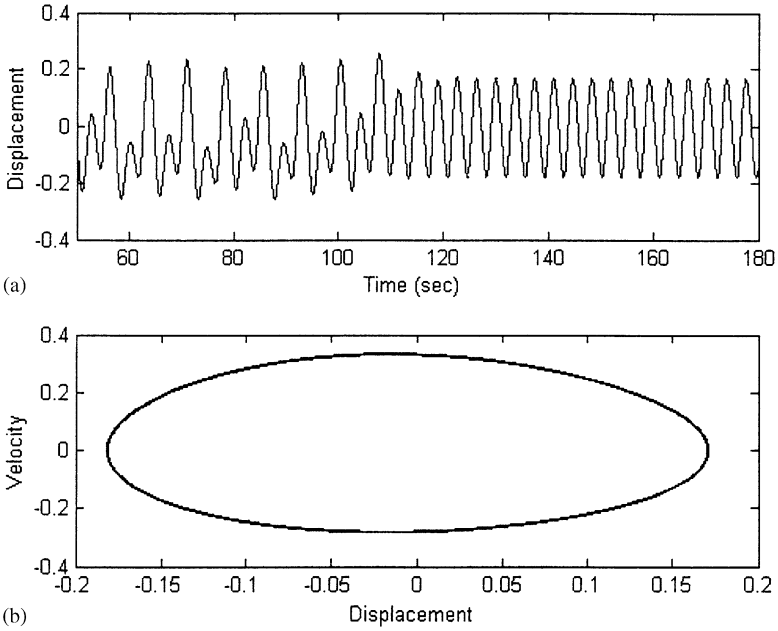

Fig. 13. Injecting a square-wave dither signal control which is used to control chaotic motion of the system for $p_0 = 3.0$ V at $\Omega = 1.708$. The dither signal ($W = 0.085$) is added after 100 s: (a) displacement time series; (b) controlled orbit.

As a result, the system equation can be written as

$$\dot{y} = \mu. \tag{22}$$

Consider the effect of the dither control added to the system equations (2) under the parameters $A_0 = 3.0$ V and $\Omega = 1.708$. By increasing the amplitude of the square-wave dither signal from $W = 0$ to 0.09, the dynamics change from chaotic behavior to periodic motion. The evolution of the bifurcation diagram is shown in Fig. 12. Now, we select the amplitude of square-wave dither $W = 0.085$. The time response of displacement is shown in Fig. 13(a) where the square-wave dither signal is added after 100 s. The chaotic behavior system is converted into a period-one orbit. The phase portrait of the controlled system is shown in Fig. 13(b).

6. Conclusions

This work is concerned with the non-linear behaviors and chaos control of a structure with a non-linear electromagnetic system using the identified non-linear model. We have examined the local stability of the theoretical solutions by studying the approximating Hill's type variational equation and we have pointed out that the analysis enables us to predict the type and the occurrence of bifurcations. In practice, the resulting criteria for bifurcations contribute to the evaluation of the operational range of a system that employs such a non-linear actuator. Furthermore, by applying the methods of harmonic balance, the Floquet theory and the

Lyapunov exponents with the assistance of numerical computations, the behaviors of a cascade of period-doubling bifurcations routes to chaos obtained from the identified mathematical model coincide with that obtained from experiments.

The presence of chaotic behavior is generic for certain non-linearities, ranges of parameters and external force, where one wishes to avoid or control so as to improve the performance of a dynamic system. The state-feedback control technique is simple and effective for chaos suppression. It can be implemented by adding the feedback of suitable variable to the original system with sufficiently high control gain to suppress the development of chaos in many generally chaotic dynamics. We can also efficiently convert the chaotic system into a periodic orbit by injecting a dither signal in front of the non-linearity of a chaotic system.

Appendix A

The coefficients, $G_1, G_2, G_3, F_0, F_1, F_2, H_0, H_1, J, \bar{\lambda}_{0-2}$, are shown as follows:

$$
\begin{aligned}
J = {} & 0.1375557253927953 + A_0 + 2.273239327084512 \times A_0^2 - 9.62585816871588 \times A_0^3 \\
& + 1.136619663542256 \times A_1^2 - 14.43878725307382 \times A_0 \times A_1^2 \\
& + 0.4349254734283934 \times B_0 - 0.865174989812019 \times B_0^2 \\
& + 1.267631885968822 \times B_0^3 - 0.955810585368086 \times B_0^4 + 0.872550216745302 \times B_0^5 \\
& - 0.884558900402063 \times B_0^6 + 0.958619077428414 \times B_0^7 - 1.088173763685085 \times B_0^8 \\
& + 1.278110432622419 \times B_0^9 - 0.4325874949060096 \times B_1^2 \\
& + 1.901447828953233 \times B_0 \times B_1^2 - 2.867431756104258 \times B_0^2 \times B_1^2 \\
& + 4.362751083726512 \times B_0^3 \times B_1^2 - 6.634191753015473 \times B_0^4 \times B_1^2 \\
& + 10.06550031299835 \times B_0^5 \times B_1^2 - 15.23443269159119 \times B_0^6 \times B_1^2 \\
& + 23.00598778720354 \times B_0^7 \times B_1^2 - 0.3584289695130323 \times B_1^4 \\
& + 1.636031656397441 \times B_0 \times B_1^4 - 4.975643814761605 \times B_0^2 \times B_1^4 \\
& + 12.58187539124793 \times B_0^3 \times B_1^4 - 28.56456129673348 \times B_0^4 \times B_1^4 \\
& + 60.3907179414093 \times B_0^5 \times B_1^4 \\
& - 0.2764246563756447 \times B_1^6 + 2.096979231874656 \times B_0 \times B_1^6 \\
& - 9.52152043224449 \times B_0^2 \times B_1^6 + 33.55039885633849 \times B_0^3 \times B_1^6 \\
& - 0.2975475135076404 \times B_1^8 + 3.145349892781734 \times B_0 \times B_1^8, \\
G_1 = {} & A_1 \times \cos(\theta_1) + 4.546478654169026 \times A_0 \times A_1 \times \cos(\theta_1) \\
& - 28.87757450614764 \times A_0^2 \times A_1 \times \cos(\theta_1) - 7.21939362653691 \times A_1^3 \times \cos(\theta_1) \\
& - A_1 \times \Omega^2 \times \cos(\theta_1), \\
G_2 = {} & -0.3317906657883207 \times A_1 \times \Omega \times \sin(\theta_1), \\
G_3 = {} & 0.4349254734283934 \times B_1 \times \cos(\theta_2) - 1.730349979624038 \times B_0 \times B_1 \times \cos(\theta_2)
\end{aligned}
$$

$$
\begin{aligned}
&+ 3.802895657906466 \times B_0^2 \times B_1 \times \cos(\theta_2) - 3.823242341472344 \times B_0^3 \times B_1 \times \cos(\theta_2)\\
&+ 4.362751083726512 \times B_0^4 \times B_1 \times \cos(\theta_2) - 5.307353402412378 \times B_0^5 \times B_1 \times \cos(\theta_2)\\
&+ 6.710333541998898 \times B_0^6 \times B_1 \times \cos(\theta_2) - 8.70539010948068 \times B_0^7 \times B_1 \times \cos(\theta_2)\\
&+ 11.50299389360177 \times B_0^8 \times B_1 \times \cos(\theta_2) + 0.950723914476617 \times B_1^3 \times \cos(\theta_2)\\
&- 2.867431756104258 \times B_0 \times B_1^3 \times \cos(\theta_2) + 6.544126625589766 \times B_0^2 \times B_1^3 \times \cos(\theta_2)\\
&- 13.26838350603094 \times B_0^3 \times B_1^3 \times \cos(\theta_2) + 25.16375078249587 \times B_0^4\\
&\times B_1^3 \times \cos(\theta_2) - 45.70329807477357 \times B_0^5 \times B_1^3 \times \cos(\theta_2)\\
&+ 80.5209572552124 \times B_0^6 \times B_1^3 \times \cos(\theta_2) + 0.5453438854658137 \times B_1^5 \times \cos(\theta_2)\\
&- 3.317095876507736 \times B_0 \times B_1^5 \times \cos(\theta_2) + 12.58187539124793 \times B_0^2\\
&\times B_1^5 \times \cos(\theta_2) - 38.08608172897797 \times B_0^3 \times B_1^5 \times \cos(\theta_2)\\
&+ 100.6511965690155 \times B_0^4 \times B_1^5 \times \cos(\theta_2) + 0.5242448079686639 \times B_1^7 \times \cos(\theta_2)\\
&- 4.760760216122247 \times B_0 \times B_1^7 \times \cos(\theta_2)\\
&+ 25.16279914225387 \times B_0^2 \times B_1^7 \cos(\theta_2) + 0.6290699785563471 \times B_1^9 \cos(\theta_2),
\end{aligned}
$$

$$F_0 = -0.6409680633837136 \times p_0 - 0.942600093211344 \times p_0 \times B_0,$$

$$F_1 = 2.784607521417466 \times B_1 \times \cos(\theta_2) + 8.19002212181608 \times B_0 \times B_1 \times \cos(\theta_2),$$

$$F_2 = -B_1 \times \Omega \times \sin(\theta_2),$$

$$H_0 = 2.784607521417466 \times B_0 + 4.095011060908039 \times B_0^2 + 2.047505530454019 B_1^2,$$

$$H_1 = 0.471300046605672 \times p_0 \times B_1 \times \sin(\theta_2),$$

$$
\begin{aligned}
\bar{\lambda}_0 = &- 1 - 4.546478654169026 \times A_0 + 28.87757450614764 \times A_0^2\\
&+ 14.43878725307382 \times A_1^2,
\end{aligned}
$$

$$\bar{\lambda}_1 = -4.546478654169026 \times A_1 + 57.75514901229528 \times A_0 \times A_1,$$

$$\bar{\lambda}_2 = 14.43878725307382 \times A_1^2.$$

References

[1] S.C. Chang, T.C. Tung, Identification of a non-linear electromagnetic system: an experimental study, *Journal of Sound and Vibration* 214 (1998) 853–872.

[2] C. Hayashi, *Non-linear Oscillations in Physical Systems*, McGraw-Hill, New York, 1964.

[3] A. Wolf, J.B. Swift, H. Swinney, J.A. Vastano, Determining Lyapunov exponents from a time series, *Physica D* 16 (1985) 285–317.

[4] E. Ott, C. Grebogi, J.A. Yorke, Controlling chaos, *Physical Review Letters* 64 (1990) 1196–1199.

[5] W.L. Ditto, S.N. Rauseo, M.L. Spano, Experimental control of chaos, *Physical Review Letters* 65 (1990) 3211–3214.
[6] E.R. Hunt, Stabilizing high-period orbits in a chaotic system: the dioderesonator, *Physical Review Letters* 67 (1991) 1953–1955.
[7] Y.C. Lai, M. Ding, C. Grebogi, Controlling Hamiltonian chaos, *Physical Review E* 67 (1993) 86–92.
[8] C. Cai, Z. Xu, W. Xu, B. Feng, Notch filter feedback control in a class of chaotic systems, *Automatica* 38 (2002) 695–701.
[9] C. Cai, Z. Xu, W. Xu, Converting chaos into periodic motion by feedback control, *Automatica* 38 (2002) 1927–1933.
[10] C.C. Fun, P.C. Tung, Experimental and analytical study of dither signals in a class of chaotic system, *Physics Letters A* 229 (1997) 228–234.
[11] W. Szemplinska-Stupnicka, *The Behavior Non-linear Vibration Systems*, Vol. I, Kluwer Academic Publishers, Dordrecht, 1990.
[12] W. Szemplinska-Stupnicka, J. Bajkowski, The 1/2 subharmonic resonance and its transition to chaotic motion in a non-linear oscillator, *International Journal of Non-linear Mechanics* 21 (1986) 401–419.
[13] C.Y. Tseng, P.C. Tung, Stability, bifurcation, and chaos of a structure with a non-linear actuator, *Japanese Journal of Applied Physics* 34 (1995) 3766–3774.
[14] W. Szemplinska-Stupnicka, G. Iooss, F.C. Moon, *Chaotic Motions in Non-linear Dynamical Systems*, Springer, New York, 1988.
[15] W. Szemplinska-Stupnicka, Bifurcation of harmonic solution leading to chaotic motion in the softening type duffing's oscillator, *International Journal of Non-linear Mechanics* 23 (1988) 257–277.
[16] J.L. Kaplan, J.A. Yorke, Chaotic Behavior of Multidimensional Difference Equations, Lecture Notes in Mathematics, Springer, New York, 1979, pp. 228–237.
[17] IMSL, Inc, User's manual—FORTRAN Subroutines for Mathematical Applications, IMSL MATH/LIBRARY, Vol. II, Chapter 5, 1989, p. 633.